PCCP

Accepted Manuscript

ROYAL SOCIETY OF CHEMISTRY

www.rsc.org/pccp

Cite this: DOI: 10.1039/c0xx00000x

www.rsc.org/xxxxxx

PAPER

Adsorption of Metal Adatoms on Single-Layer Phosphorene

Vadym V. Kulish,*[a,b] Oleksandr I. Malyi,[c] Clas Persson[c,d] and Ping Wu*[a]

Received (in XXX, XXX) Xth XXXXXXXXX 20XX, Accepted Xth XXXXXXXXX 20XX
DOI: 10.1039/b000000x

Single- or few-layer phosphorene is a novel two-dimensional direct-bandgap nanomaterial. Based on first-principles calculations, we present a systematic study on binding energy, geometry, magnetic moment and electronic structure of 20 different adatoms adsorbed on phosphorene. The adatoms cover a wide range of valences, including *s* and *p* valence metals, 3*d* transition metals, noble metals, semiconductors, hydrogen and oxygen. We find that adsorbed adatoms produce a rich diversity of structural, electronic and magnetic properties. Our work demonstrates that phosphorene forms strong bonds with all studied adatoms while still preserving its structural integrity. The adsorption energies of adatoms on phosphorene are more than twice larger than on graphene, while the largest distortions of phosphorene are only ~0.1-0.2 Å. The charge carrier type in phosphorene can be widely tuned by adatom adsorption. The unique combination of high reactivity with good structural stability is very promising for potential applications of phosphorene.

Introduction

Two-dimensional (2D) nanomaterials (*e.g.* graphene, BN, MoS_2, WSe_2, etc.) have attracted tremendous research attention recently. Their unusual properties, originating from the quantum size effects, have led to many promising applications in nanoelectronics, catalysis and energy storage.[1-7] Single-layer phosphorus (*"phosphorene"*) is a new material in the family of 2D nanostructures. It can be obtained by a mechanical exfoliation of the black phosphorus, which is a stable compound with a natural layered structure. Very recently, phosphorene with a thickness of only few nanometers has been produced by several groups worldwide.[8-11] Inside phosphorene layer, each P atom is bonded with three neighboring P atoms, forming a puckered honeycomb structure similar to graphene. However, unlike zero-bandgap graphene, phosphorene is a direct band gap semiconductor (0.3 eV in the bulk form) which makes it very attractive for the nanoelectronic devices.[12] Indeed, phosphorene-based transistors demonstrate high on/off ratios (>10^5) and high carrier mobilities (300-1000 $cm^2 V^{-1} s^{-1}$).[8, 9, 13, 14] Furthermore, phosphorene shows a *p*-type or ambipolar behavior in field-effect transistors.[8, 9] Consequently, it is possible to fabricate 2D CMOS inverters using phosphorene as the *p*-channel and MoS_2 as the *n*-channel.[15] Besides, the unique anisotropic structure of phosphorene leads to a highly anisotropic electronic and optical behavior, stress/strain response, etc.[16-26] Electrons and phonons act in a highly anisotropic manner within the phosphorene layer allowing for the realization of novel electronic, optoelectronic and nanomechanical devices.[27-31]

While many unique features of phosphorene have been pointed out recently, many more fascinating properties are yet to be discovered. Furthermore, there are fundamental questions that have to be answered before the application of phosphorene in practical devices. For instance, what is the chemical reactivity of phosphorene? How does phosphorene react with adsorbed atoms and molecules? What are the possible doping strategies to engineer the electronic properties of phosphorene? Motivated by the above issues, we present a detailed first-principles study on the structural, magnetic and electronic properties of 20 adatoms adsorbed on single-layer phosphorene. The results of our study may be interesting from the prospects of both fundamental science of phosphorene and its potential applications. For instance, adsorption of hydrogen and oxygen on phosphorene can tell about its surface reactivity and whether phosphorene can be oxidized. Adsorption of alkali atoms can be used as an efficient approach to produce high electron sheet densities, as has been previously shown by K doping in MoS_2 and WSe_2 transistors.[32, 33] The reaction with Li and Na atoms is relevant for the potential application of phosphorene in Li-ion and Na-ion batteries.[34] The atomic decoration[35] is an efficient way to produce nanomaterials for hydrogen storage,[36-39] nanocatalysts,[40-42] spin devices,[43-45] etc. In this paper, the main trends in adsorption energy, geometry, magnetic moment and electronic density of states (DOS) of adatoms on phosphorene are predicted. The adatoms cover a range of valences, including *s* and *p* valence metals, transition metals, noble metals, semiconductors, hydrogen and oxygen. We find that adsorption of adatoms produces a wide variety of electronic, magnetic and structural properties. Our study demonstrates that phosphorene forms strong bonds with all adatoms while still preserving its structural integrity. The adsorption energies of adatoms on phosphorene are more than twice larger than on graphene, while maximum distortions of phosphorene lattice are about 0.1-0.2 Å. This unique combination of high reactivity with good structural stability is very promising for potential applications of phosphorene. With the availability of

synthesized single- and few-layer phosphorene, our theoretical study can further enhance the knowledge about its properties and explain its experimental behavior in various potential applications.

Computation Methods

First-principles calculations are performed within the density-functional theory (DFT) framework, as implemented in Quantum Espresso package.[46] The electron-ion interaction is described by a projector augmented wave (PAW) method[47] using Perdew-Burke-Ernzerhof (PBE) pseudopotentials.[48] The kinetic-energy cutoff for valence electron wave functions is set as 35 Ry (476 eV). The Marzari-Vanderbilt cold smearing with a smearing factor of σ = 0.005 Ry (0.07 eV) is used in all calculations. The optimized structures are obtained by relaxing all atomic positions using the Broyden-Fletcher-Goldfarb-Shanno (BFGS) quasi-Newton algorithm until all forces are smaller than 0.01 eV/Å. With the selected modeling parameters, the predicted lattice constants and cohesive energies for all elements agree well with the experimental data. The amount of charge transfer between the adsorbed atom and phosphorene is estimated from the grid-based Bader charge analysis.[49]

To model adatom-phosphorene structure, we use an orthorhombic supercell ($\alpha = \beta = \gamma = 90°$) with periodic boundary conditions. In our notation, the x and y directions are parallel and the z direction is perpendicular to the phosphorene plane. Vacuum spacing of 20 Å in the z direction is used to prevent the interaction of the single-layer phosphorene with its periodic images. A large (3×4) supercell of phosphorene is used (containing 48 P atoms), giving the nearest adatom-adatom distance of ~13.2 Å. In such way, adatom-adatom interaction can be neglected and the interaction of isolated adatom with phosphorene can be studied. The Brillouin zone for a (3×4) supercell is sampled by 5×5×1 and 24×24×1 k-points grids for atomic optimization and electronic structure calculations, respectively. The total energy of an isolated atom is calculated for a single atom in a cubic supercell of side length 20 Å. Only the Γ point of the Brillouin zone is used in such case.

Results and Discussion

Atomic structure of single-layer phosphorene

Single-layer phosphorene can be produced by mechanical exfoliation of black phosphorus (BP) – a stable compound, structurally similar to graphite.[8-10, 12] As shown in Figure 1a, BP has a layered structure with weak van der Waals forces between the layers and strong in-plane covalent interactions. The atomic structure of single-layer phosphorene is shown in Figure 1b. It has a hexagonal (honeycomb) structure with each P atom covalently bonded to three neighbors, similar to graphene. However, phosphorene layer is not flat; instead, it forms a puckered surface due to the sp^3 hybridization. The optimized lattice parameters for single-layer phosphorene are a = 4.62 Å and b = 3.30 Å. The calculated puckering height (*i.e.* thickness of single layer) is 2.10 Å. The calculated P-P bond lengths are 2.22 Å for the horizontal bonds and 2.26 Å for the bonds in other directions. The sum of bond angles at each P atom in phosphorene is equal to 304.28°, close to the idealized value of 328° for sp^3 (tetrahedral) configuration and much smaller than 360° for sp^2 (planar).

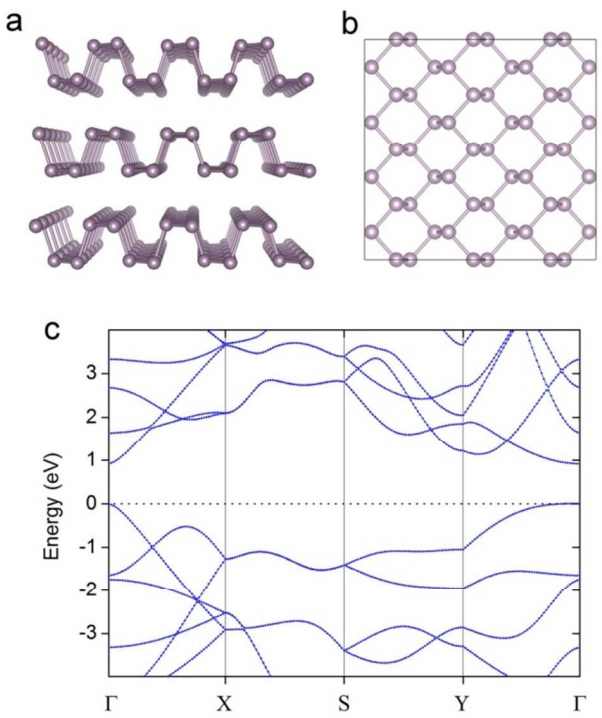

Fig. 1 Crystal structure of (a) bulk black phosphorus (side-view), and (b) single-layer phosphorene (top-view); (c) electronic band structure of single-layer phosphorene along Γ→X→S→Y→ Γ direction. Zero energy value corresponds to the VBM

The calculated band structure of single-layer phosphorene is shown in Figure 1c. Phosphorene is a semiconductor with a calculated direct band gap of 0.80 eV, consistent with recent GGA-PBE studies.[16, 17, 50] Our calculated band gap value is close to the experimentally measured transport band gap of 1.0-1.5 eV for the single-layer phosphorene.[9, 14] The valence band maximum (VBM) and the conduction band minimum (CBM) are both located at the Γ point. The calculated band structure shows highly anisotropic electronic properties of single-layer phosphorene. We can notice distinctly different band dispersions along the Γ→Y and Γ→X directions for both valence and conduction bands. Note that Γ→Y and Γ→X correspond to zigzag and armchair orientations of phosphorene in real space, respectively. Since effective mass of electrons (m_e) and holes (m_h) is inversely proportional to the band curvature, it also becomes highly anisotropic – heavy along the zigzag and light along the armchair direction. This explains the recent electrical transport measurements where the drain current and Hall mobility have been twice as larger in one direction over another in few-layer black phosphorus.[9] The presence of direct band gap in phosphorene is crucial and clearly distinguishes it from the other 2D materials, such as graphene and silicene.

The work function (Φ) of single-layer phosphorene is defined as[51, 52]:

$$\Phi = E_{vacuum} - E_F \quad (1)$$

where E_{vacuum} is the reference vacuum energy and E_F is the Fermi level energy. Since phosphorene is a semiconductor, we set E_F at the midgap.[51] The exact value of E_{vacuum} is taken as the average electrostatic potential in the vacuum region far from the phosphorene surface where it approaches a constant. On this purpose, we use macroscopic averages technique. Our calculated work function of pristine single-layer phosphorene is equal to 4.60 eV.

Adsorption energy and geometry

The adsorption (binding) energy (E_a) of adatom on single-layer phosphorene is defined as

$$E_a = E_{A+P} - E_P - E_A \quad (2)$$

where E_{A+P}, E_P and E_A are the total energies of adatom-phosphorene system, pristine phosphorene and isolated atom, respectively. The 3×4 supercell of phosphorene is used in our calculations corresponding to the size of 13.86×13.20 Å (48 P atoms). We consider four high-symmetry sites for adatom adsorption, as shown in Figure 2: (1) *H* site above the P_6 hexagon, (2) *B* above the middle-point of *bottom* P-P bond, (3) *B1* above the middle-point of *top* P-P bond, and (4) *T* on top of the P atom. The P-P bond in the atomic plane nearer to adatom is denoted as "top". To find the equilibrium adatom-phosphorene structure, we initially put adatoms at each adsorption site, and then relax all the atomic coordinates in the system. From our definition, the negative value of E_a shows that a given adatom-phosphorene system is stable. The large absolute value of E_a energy means strong interaction between adatom and phosphorene. The adsorption site with the largest adsorption energy (minimum total energy) is referred to as the most favorable. A summary of the obtained results is shown in Table 1.

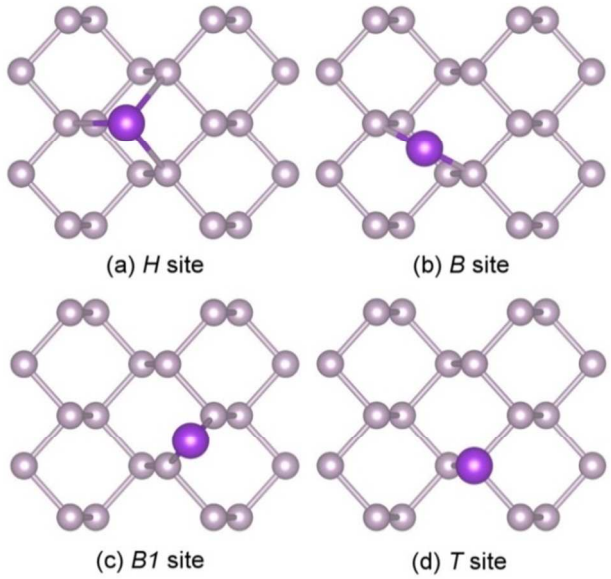

Fig. 2 Typical adatom adsorption sites on phosphorene: (a) *H*, (b) *B*, (c) *B1*, and (d) *T*

Table 1 Calculated structural and magnetic properties for single atoms adsorbed on (3x4) phosphorene at the most favourable adsorption sites. Adsorption energies (E_a); minimum adatom-phosphorus (A-P) distances; the net magnetic moments (μ) (where NM refers to non-magnetic system, while the value in the brackets indicates the magnetic moment of the free atom); phosphorene distortion (Δz_{max}), calculated as the largest displacement in *z* direction of P atoms from their initial positions

Adatom	Site	E_a (eV)	d(A-P) (Å)	μ (μ_B)	Δz_{max} (Å)
Li	*H*	-1.88	2.50	NM	0.11
Na	*H*	-1.31	2.84	NM	0.10
K	*H*	-1.61	3.20	NM	0.10
Cu	*H*	-2.18	2.23	NM	0.14
Ag	*H*	-1.13	2.45	0.02	0.10
Au	*H*	-1.61	2.37	0.72	0.09
Pd	*H*	-3.48	2.27	NM	0.11
Pt	*H*	-4.71	2.23	NM	0.13
Ti	*H*	-3.41	2.40	2.00 (3)	0.29
V	*H*	-2.68	2.39	3.99 (5)	0.14
Cr	*H*	-1.66	2.39	4.93 (6)	0.13
Mn	*H*	-1.78	2.22	3.00 (5)	0.18
Fe	*H*	-2.70	2.18	2.00 (4)	0.11
Co	*H*	-3.56	2.13	1.00 (3)	0.25
Ni	*H*	-4.09	2.12	0.00 (2)	0.14
Si	*B*	-2.66	2.29	NM	0.21
Ge	*B*	-2.22	2.40	NM	0.18
P	*B*	-2.02	2.17	NM	0.12
H	*T*	-1.29	1.45	1.00	0.30
O	*T*	-2.06	1.50	NM	0.11

Alkali adatoms (Li, Na and K) prefer to adsorb at the *H* site of phosphorene. Such behavior is typical for the ionic impurities which usually favor adsorption sites of high coordination on semiconductor/metal surfaces. The largest adsorption energy of -1.88 eV and the smallest bond length of 2.50 Å are found for the adsorption of Li atom. Interestingly, the adsorption energy of alkali adatoms on phosphorene does not follow the trend in adatom atomic size. Among alkalis, Li shows the largest adsorption energy, while Na – the lowest. Because of the small electron affinities of alkali atoms, they transfer electrons to phosphorene. The Bader charge analysis shows that 0.89, 0.84 and 0.86 |*e*| is transferred from Li, Na and K, respectively. The large adsorption energy of alkali atoms is an advantage of phosphorene over graphene. It has been argued that monolayer graphene may not be suitable as anode for Li-ion batteries due to unfavorable Li-graphene binding and tendency of Li atoms to cluster together.[53, 54] The improved battery performance can be achieved in graphene either by introducing edges, defects, or nitrogen/boron doping.[55-57] In contrast, we find that Li and Na can readily bind to phosphorene even without any special defect/doping treatment. Moreover, the calculated Li and Na adsorption energies are larger than their bulk cohesive energies, suggesting the Li and Na would form 2D layers on phosphorene rather than cluster together. The structural distortions in phosphorene caused by alkali adsorption are small. For instance, the maximum vertical displacement of P atoms is only ~0.1 Å. These results show a high potential of phosphorene as anode material for Li- or Na-ion batteries.

The 3*d* transition metals (Ti, V, Cr, Mn, Fe, Co, Ni) produce a diverse variety of adsorption energies and magnetic properties on phosphorene. All adatoms prefer the *H* site, and form strong covalent bonds with phosphorene. The adsorption energies range from -1.66 (Cr) to -3.41 (Ti) and -4.09 eV (Ni). These values are much larger than adsorption energies of TM adatoms on graphene (-0.10…-1.95 eV)[58-61] implying much stronger interaction between TMs and phosphorene. The maximum adsorption energies correspond to Ti and Ni adatoms which have d^2 and d^8 electronic configurations, respectively. The weakest binding has been found for Cr and Mn adatoms having half-filled *d*-shells. Most of the transition metals adsorbed on phosphorene have a magnetic moment. Across the series from Ti to Ni, the magnetic moment forms a "volcano" curve with the maximum value at Cr atom. When adsorbed on phosphorene, the magnetic moments of all TM adatoms are reduced by 1-2 μ_B from their free atom states. The reduction is attributed to the transfer of spin-polarized electrons from adatom to phosphorene, whose states are not spin-polarized. The reduction of the magnetic moment may be also caused by the promotion of the 4*s* electrons of TMs into 3*d* orbitals.[62] Interestingly, the Ni adatom, which is magnetic in bulk state, shows no magnetism when adsorbed on phosphorene. Similar trends have been observed for carbon nanostructures.[58-61] The analysis of isosurface spin density has been performed in order to examine the origin and distribution of magnetism in TM-phosphorene. We find that the total magnetic moment of the system mainly comes from the TM atom with a little contribution from its nearest neighbors, as shown in Figure S2.

Recent studies demonstrate that magnetic adsorbates on graphene can lead to unusual quantum phase phenomena such as Kondo effect.[63, 64] It is interesting to investigate the possibility of implementation of Kondo effect in TM-chemisorbed phosphorene. Moreover, phosphorene would have an advantage over graphene in terms of much stronger TM-P binding providing the chemical route to produce localized magnetic moments even at moderate temperatures.

Metal-phosphorene interaction is a subject of particular interest due to its relevance for electrode-channel interface in phosphorene-based nanoelectronic devices. Besides, functionalization with Pt and Pd nanoparticles has been widely used to produce hybrid nanostructures for catalysis.[65, 66] For both applications, the strong contact between phosphorene and metal is desirable. Our calculations show that the metal adatoms can be divided into two distinct subgroups: Pd, Pt, Ti and Ni form strong bonds with phosphorene ($E_a \approx$ -3…-4 eV), while Au and Ag – relatively weaker ($E_a \approx$ -1 eV). The difference in reactivity of metals can be related to their electronic structure. Ag and Au have *d* bands which are fully filled and do not cross the Fermi level, leading to a weak interaction with many supports.[67] In Pt and Pd, two *d* bands cross the Fermi level, enhancing the chemical reactivity. Moreover, when Pd atoms are involved in chemical bonds, the *sp*-band typically becomes partially filled at the costs of the *d*-band occupancy.[68] Consequently, Pd and Pt adatoms are more reactive. Interestingly, we find the spin-polarized ground state for Ag and Au single adatoms on phosphorene with small magnetic moments of 0.02 and 0.72 μ_B, respectively. The magnetism in Au-phosphorene mainly comes from the Au *s* and *p* states. Our analysis shows that spin-polarized peaks that appear near to the Fermi level mainly come from *s* and *p* orbitals (Figure S5). However, when Au_2-dimer is adsorbed on phosphorene, the magnetic moment becomes zero. Moreover, the Au_2-dimer is more stable than Au single adatom by about 0.35 eV per atom, suggesting that experimentally synthesized Au-phosphorene samples may be non-magnetic. We find a crossover between electron donating (Cu, Ag) and electron accepting (Au) behavior. This is similar to the recent experimental reports on the hole doping in Au-deposited graphene.[69] The Bader charge analysis shows the charge of +0.32, +0.25 and -0.15 |*e*| on Cu, Ag and Au adatoms, respectively. Among all studied metal adatoms, Au and Pt act as electron acceptors. This result suggests that Au or Pt adsorption can be used as an effective way to produce *p*-type doping of phosphorene.

We can notice that the adsorption energy of metal adatoms on phosphorene is twice larger than on graphene and even CNTs. This can be attributed to the difference in atomic structures of materials. Carbon atoms in graphene form robust sp^2 network where each carbon atom has three σ and one π orbitals. The adatom chemisorption on graphene involves the breaking of one of the π bonds and transformation from sp^2 to sp^3 local symmetry, which is energetically costly. Phosphorene, on the other side, already has sp^3 hybridization which is more reactive than sp^2.

We examine the distortions due to adatom adsorption by calculating the largest displacement in *z* direction (Δz_{max}) of P atoms from their initial positions. As shown in Table 1, typical values of Δz_{max} in phosphorene are about 0.1 Å. Although larger than in graphene, the deformations are smaller or comparable to other materials. For instance, the deformation from circular tube as measured by the aspect ratio (r_{max}/r_{min}) is 10% in Li-adsorbed CNTs.[70] The displacements of Si atoms in silicene due to metal adsorption can reach up to 0.68 Å, which is even larger than silicene thickness (*i.e.* buckling height) of 0.46 Å.[71] This suggests that phosphorene has a better stability than silicene.

Adatoms from group IVA (Si and Ge) prefer adsorption at the *B* site. The adsorption energy of Si is equal to -2.26 eV with the Si-P bond length of 2.29 Å. The adsorption of Si and Ge leads to a hybridization of adatom *p* orbitals with the *p* orbitals of phosphorene due to the formation of covalent bonds. The previous studies have shown that the bridge site is also the most energetically favorable for Si, Ge adatoms on graphene.[72] P adatom also favors adsorption at the B site, similarly to the covalent impurities from Group IVA. The adsorption energy of P adatom on phosphorene is -2.02 eV and the minimum P_{ad}-P distance is 2.17 Å, slightly shorter than P-P bond lengths in phosphorene (2.22-2.26 Å).

We find that O adatom prefers to adsorb at the *T* site. When initially placed at the *H* or *B* position, O atom still relaxes to the *T* site. The adsorption energy is equal to -2.06 eV and minimum O-P distance is 1.50 Å. The calculated bond length is much shorter than the sum of the P (1.07 Å) and O (0.66 Å) covalent radii,[73] which suggests bonding beyond a single σ bond and, possibly, formation of P=O double bond. Furthermore, the calculated bond length in O-phosphorene matches precisely the experimental P=O double bond length of 1.51 Å in phosphoric acid.[74] The short P-O bond may result from the transfer of electrons from lone pair,[20] associated with each P atom. Since oxygen has the second highest electronegativity in the periodic table (3.44 on Pauling scale), it is

expected to withdraw a significant amount of charge from phosphorene. Indeed, Bader charge analysis shows that 1.88 $|e|$ is transferred from P to O during oxygen adsorption, and the charge is mainly transferred from the P atom forming the bond with O. Such interaction between P and O is rather unique since the formation of double bonds with oxygen has not been observed in graphene, silicene or MoS_2.[42, 75-77] The strong P-O binding explains the experimentally observed fast degradation of layered black phosphorus when exposed to air.[13, 78]

As a monovalent atom, H prefers to adsorb at the *T* site. The calculated adsorption energy is -1.29 eV. The optimized P-H bond length is 1.45 Å, close to the experimental bond length of 1.42 Å in phosphine (PH_3). The chemisorption of H atom leads to a vertical displacement of hydrogenated P atom by 0.30 Å. All other P atoms remain close to their original positions ($\Delta z < 0.1$ Å). Single H atom adsorbed on phosphorene possesses a magnetic moment of 1.00 μ_B. In order to examine the stability of magnetic state, we increase H concentration by placing the second H atom on phosphorene. According to the basic functionalization principles, chemisorption of next H atom is more favorable when it leads to minimal additional atomic distortions.[79] Thus the most energetically stable is configuration with two H atoms at the same P-P bond but from different sides of phosphorene plane. We find that the magnetic moment becomes zero in such case. These results are consistent with the recent theoretical works on hydrogenation of graphene.[79-81]

The character of binding between adatoms and phosphorene can be examined by calculating the charge-density difference ($\Delta\rho$) as:

$$\Delta\rho = \rho_{A+P} - \rho_P - \rho_A \quad (3)$$

where ρ_{A+P}, ρ_P and ρ_A are total charge densities of adatom-phosphorene system, pristine phosphorene and isolated adatom, respectively, with P and A atoms in the exact same positions as they occupy in A+P system. Figure 3 shows the $\Delta\rho$ isosurfaces for Li, P and O adsorption. For Li (Figure 3a), the charge is mainly transferred from alkali atom to P. In case of covalent bonding (Figure 3b), the charge is accumulated in the middle of A-P bonds. For O (Figure 3c), the charge is transferred from P to O. The direction of charge transfer can be understood from the electronegativities of the elements (0.98, 2.19 and 3.44 on the Pauling scale for Li, P and O, respectively).

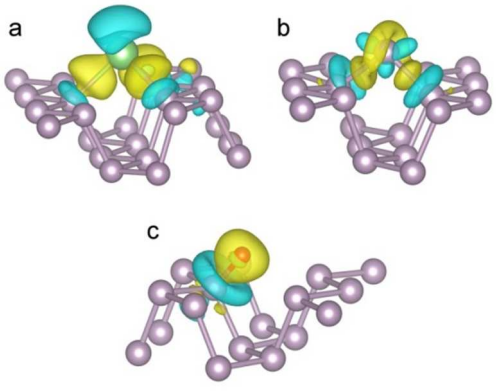

Fig. 3 Charge density difference isosurfaces for the representative adatom-phosphorene systems. (a) Ionic Li-P bonding (charge transfer from Li to P). (b) Covalent P-P bonding (charge transfer to the middle of P-P bonds). (c) O-P bonding (charge transfer from P to O). Yellow and blue regions refer to electron accumulation and depletion, respectively

Overall, our study demonstrates that phosphorene forms strong bonds with all adatoms while still preserving its structural integrity. This is a tremendous advantage over its main 2D competitors – graphene and silicene. Graphene is very robust and stable material, but its surface reactivity is quite low. Graphene is chemically inert, does not undergo rapid chemical reactions and, thus, is used as an anti-oxidation or anti-corrosion protective layer.[82] Recent studies suggested the absence of a strong contact between semiconductor nanoparticles and pristine graphene support, unless aromatic linkers or carbon defects are introduced.[83, 84] On the other hand, single-layer silicene is very reactive, but the adatom adsorption leads to large deformations and even local reconstructions.[71, 85, 86] In contrast, phosphorene combines both high reactivity and fair stability. Specifically, the adsorption energies of adatoms to phosphorene are more than twice larger than to graphene, while typical deformations of phosphorene lattice are only 0.1-0.2 Å. The unique combination of high reactivity with good structural stability is very promising for potential applications of phosphorene.

Electronic structure

The electronic structure of phosphorene is distinctly different from its single-layer analogues (*e.g.* graphene and silicene – semimetals with a Dirac point), because it possess intrinsic band gap. Consequently, there is a wider range for electronic structure tuning in phosphorene: the adsorbed atoms can form states inside valence or conduction bands, as well as localized peaks in the middle of band gap. We examined the effects of adatoms on the electronic properties of phosphorene by calculating the total and projected densities of states (DOS). In the Figures 4-5, we present the main trends in the DOS on the examples of representative adatom-phosphorene structures from each group of adsorbants. Figure 4a shows the DOS of pristine phosphorene for a reference.

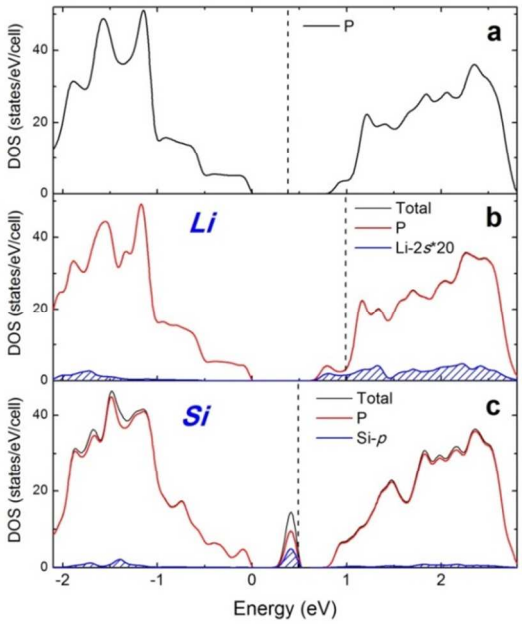

Fig. 4 Electronic density of states (DOS) of (a) pristine, (b) Li-, and (c) Si-phosphorene. The Li-2*s* states are magnified for a better convenience. The zero energy corresponds to the VBM. The dashed vertical line indicates the Fermi level

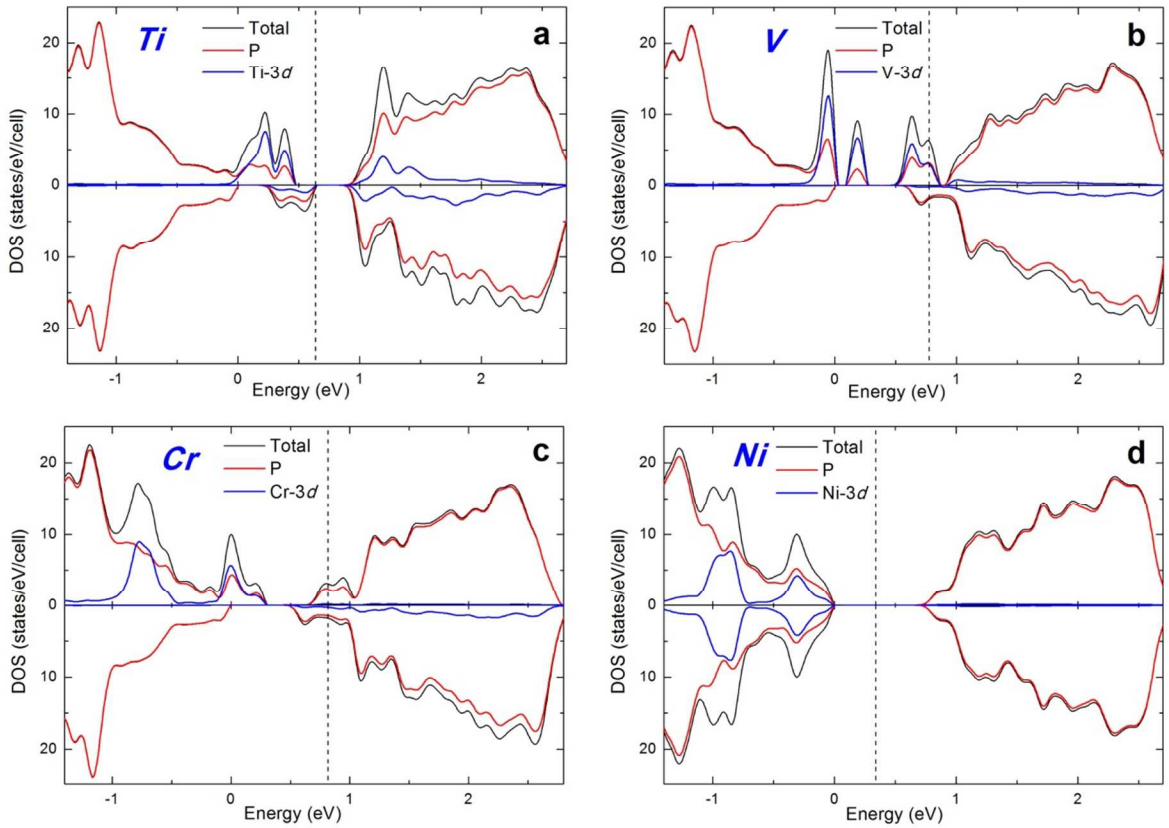

Fig. 5 DOS of (a) Ti-, (b) V-, (c) Cr- and (d) Ni-phosphorene. The zero energy corresponds to the VBM for minority-spin. The dashed vertical line indicates the Fermi level

Figure 4b shows the total density of states (DOS) of phosphorene with the adsorbed Li, which is a typical alkali adatom. The adsorption of alkali atoms does not significantly change the overall DOS of the phosphorene. Li makes two main contributions to the total DOS: one is located around the Fermi level in the conduction band, while the other is deep in the valence band as shown in Figure 4b. Because of its low ionization energy, the 2*s* valence electron of Li is donated to the phosphorene to occupy the empty conduction band. Due to the charge transfer (~0.89 |e| from Bader charge analysis), the Fermi level is shifted to the bottom of the conduction band. These results suggest that the bonding between an alkali atom and phosphorene is mainly ionic (alternatively, can be treated as covalent polar). The DOS of Na- and K-phosphorene shows similar features to Li and is shown in the supporting information.

Adatoms from Group IVA (Si and Ge) form covalent bonds with phosphorene. Due to the strong interaction, the adsorption of these adatoms produces large changes in the electronic structure of phosphorene. Figure 4c shows the DOS for Si on the *B* site. The covalently bond impurity causes a characteristic localized state in the middle of band gap. The midgap peak mainly comes from 3*p* orbitals of Si and 3*p* orbitals of phosphorene. The strong hybridization of Si and P states demonstrates the formation of covalent bonds. Highly localized impurity peak (*i.e.* flat impurity band) can be attributed to the large supercell size and, hence, negligible adatom-adatom interaction.

In order to understand the magnetism and position of the TM-atom *d* states, the DOS has been plotted for TM-phosphorene in Figure 5. Despite their low concentration, the TM atoms modify the electronic structure of phosphorene drastically. The DOS for Ti at the *H* site is shown in Figure 5a. The strong interaction between Ti and phosphorene is evident from the large hybridization between Ti and P states for both majority (spin-up) and minority (spin-down) contributions. The Ti 3*d* states are located in the midgap, as well as in the conduction band. Due to the presence of Ti midgap peaks, the band gap of Ti-phosphorene is reduced from 0.80 to 0.41 eV for spin-up and 0.20 eV for spin-down states.

For V and Cr, most impurity bands are almost completely spin-polarized, leading to the largest magnetic moment (3.99-4.93 μ_B) among the TMs on phosphorene. The V and Cr states are split into distinct groups of spin-up and spin-down states as shown in Figure 5b and 5c, respectively. The spin-up Cr 3*d* states are further split into two peaks: one is located in the valence band, and the other forms impurity state in the midgap. Both spin-up peaks are completely filled. Spin-down Cr 3*d* states are only present in the conduction band. The V states are more strongly hybridized with phosphorene states than their Cr counterparts, as also evidenced from the larger adsorption energy of V atom (-2.68 and -1.66 eV for V and Cr, respectively). The spin-up V peaks are split into two peaks and a broader state near the Fermi level, which are all hybridized with phosphorene states. The spin-

up V 3*d* states dominate the region near Fermi level. The magnetic moments coincide well with the splitting between spin-up and spin-down 3*d* states. In particular, we find that the splitting is the largest for Cr, Mn and smaller for Ti, Fe and Co. The DOS of Ni adatom at *H* site (Figure 5d) has no spin-polarization, consistent with the zero magnetic moment. Interestingly, the Ni adatom, which is magnetic in bulk state, shows no magnetism when adsorbed on phosphorene. The Ni 3*d* states are hybridized with P 3*p* states at the top of the valence band. All adsorbed TM atoms (Ti-Ni) have partially filled d states and a finite density of states at the Fermi level.

Conclusions

In this work, we present a systematic study on adsorption energy, geometry, magnetic moment and electronic structure of 20 different adatoms on single-layer phosphorene.

We find that electronic structure and charge carrier type in phosphorene can be widely tuned by adsorbed adatoms. Certain adatoms (such as Ni, Cu, Ag, Pd and Pt) form electrically inactive states, which are located entirely outside the band gap. The covalent adatoms (Si, Ge, P) form a characteristic localized midgap peak. Transition metals (Ti, V, Cr, Mn, Fe and Co) form spin-polarized states across the entire band gap region, as well as peaks in the valence and conduction bands. The alkali adatoms (Li, Na and K) preserve the original electronic structure of phosphorene, but shift the Fermi level into the conduction band. Li, Na and K adatoms transfer large amount of charge to phosphorene, and, hence, can be used for *n*-doping. In contrast, Au and Pt adatoms act as electron acceptors suggesting that Au or Pt decoration can be used to produce *p*-type doping of phosphorene.

Interestingly, we find that O forms very strong, polarized and short bonds with single-layer phosphorene (E_a = 2.06 eV and d_{min}(O-P) = 1.50 Å). The calculated bond length is much shorter than the sum of the P (1.07 Å) and O (0.66 Å) covalent radii, which suggests bonding beyond a single σ bond and, possibly, formation of P=O double bond. This is intriguing and distinctly different from graphene, silicene and MX_2 where the formation of double bonds with O has not been observed.

Importantly, phosphorene forms strong bonds with all studied adatoms while still preserving its structural integrity. This is a tremendous advantage over its main 2D competitors – graphene and silicene. Graphene is very robust and stable material, but its surface reactivity is quite low. On the other hand, single-layer silicene is very reactive, but the adatom adsorption leads to large deformations and even local reconstructions. In contrast, phosphorene combines both high reactivity and fair stability. Specifically, the adsorption energies of adatoms on phosphorene are more than twice larger than on graphene, while maximum atomic displacements in phosphorene lattice are only 0.1-0.2 Å. The unique combination of high reactivity with good structural stability is very promising for potential applications of phosphorene. The results of our study may provide understanding of the properties of phosphorene. Our work may inspire further experimental and theoretical works on phosphorene in the fields of energy storage, catalysis, sensing, nanoelectronics, and so on.

Acknowledgements

The authors appreciate the computational support received from the Singapore University of Technology and Design and the Institute of High Performance Computing (IHPC) of A*STAR of Singapore. O.I.M. and C.P. acknowledge the support from the Research Council of Norway (contract no. 221469). V.V.K. is thankful to Huang Wei for useful discussions.

Notes and references

[a] *Entropic Interface Group, Singapore University of Technology and Design, 20 Dover Drive, Singapore 138682, Singapore; E-mails: vadym_kulish@sutd.edu.sg (V.V.K.), wuping@sutd.edu.sg (P.W.)*
[b] *Institute of High Performance Computing, 1 Fusionopolis Way, #16-16 Connexis, Singapore 138632, Singapore*
[c] *Centre for Materials Science and Nanotechnology, and Department of Physics, University of Oslo, NO-0316 Oslo, Norway*
[d] *Department of Materials Science and Engineering, Royal Institute of Technology, SE-100 44 Stockholm, Sweden*

† Electronic Supplementary Information (ESI) available: Calculation details, spin density distribution and additional density of states (DOS) figures. See DOI: 10.1039/b000000x/

1. K. S. Novoselov, V. I. Falko, L. Colombo, P. R. Gellert, M. G. Schwab and K. Kim, *Nature*, 2012, **490**, 192-200.
2. A. K. Geim, *Science*, 2009, **324**, 1530-1534.
3. B. Radisavljevic, A. Radenovic, J. Brivio, V. Giacometti and A. Kis, *Nat. Nanotechnol.*, 2011, **6**, 147-150.
4. X. Huang, Z. Y. Zeng and H. Zhang, *Chem. Soc. Rev.*, 2013, **42**, 1934-1946.
5. C. Huang, C. Li and G. Shi, *Energy Environ. Sci.*, 2012, **5**, 8848-8868.
6. W. Yuan and G. Shi, *J. Mater. Chem. A*, 2013, **1**, 10078-10091.
7. Y. Ma, Y. Dai, M. Guo, C. Niu, Y. Zhu and B. Huang, *ACS Nano*, 2012, **6**, 1695-1701.
8. L. Li, Y. Yu, G. J. Ye, et al., *Nat. Nanotechnol.*, 2014, **9**, 372-377.
9. H. Liu, A. T. Neal, Z. Zhu, Z. Luo, X. Xu, D. Tománek and P. D. Ye, *ACS Nano*, 2014, **8**, 4033-4041.
10. M. Buscema, D. J. Groenendijk, S. I. Blanter, G. A. Steele, H. S. J. van der Zant and A. Castellanos-Gomez, *Nano Lett.*, 2014, **14**, 3347–3352.
11. W. Lu, H. Nan, J. Hong, et al., *Nano Res.*, 2014, **7**, 853-859.
12. H. O. H. Churchill and P. Jarillo-Herrero, *Nat. Nanotechnol.*, 2014, **9**, 330-331.
13. S. P. Koenig, R. A. Doganov, H. Schmidt, A. H. C. Neto and B. Ozyilmaz, *Appl. Phys. Lett.*, 2014, **104**, 103106.
14. S. Das, W. Zhang, M. Demarteau, A. Hoffmann, M. Dubey and A. K. Roelofs, *Nano Lett.*, 2014, **14**, 5733–5739.
15. Y. Deng, Z. Luo, N. J. Conrad, et al., *ACS Nano*, 2014, **8**, 8292-8299.
16. R. Fei and L. Yang, *Nano Lett.*, 2014, **14**, 2884–2889.
17. A. S. Rodin, A. Carvalho and A. H. Castro Neto, *Phys. Rev. Lett.*, 2014, **112**, 176801.
18. V. Tran and L. Yang, *Phys. Rev. B*, 2014, **89**, 245407.
19. T. Hong, B. Chamlagain, W. Lin, H.-J. Chuang, M. Pan, Z. Zhou and Y.-Q. Xu, *Nanoscale*, 2014, **6**, 8978-8983.
20. A. N. Rudenko and M. I. Katsnelson, *Phys. Rev. B*, 2014, **89**, 201408.
21. H. Guo, N. Lu, J. Dai, X. Wu and X. C. Zeng, *J. Phys. Chem. C*, 2014, **118**, 14051–14059.
22. J. Qiao, X. Kong, Z.-X. Hu, F. Yang and W. Ji, *Nat. Commun.*, 2014, **5**, 4475.

23. F. Xia, H. Wang and Y. Jia, *Nat. Commun.*, 2014, **5**, 4458.
24. Q. Wei and X. Peng, *Appl. Phys. Lett.*, 2014, **104**, 251915.
25. X. Han, H. M. Stewart, S. A. Shevlin, C. R. A. Catlow and Z. X. Guo, *Nano Lett.*, 2014, **14**, 4607-4614.
26. W. Li, G. Zhang and Y.-W. Zhang, *J. Phys. Chem. C*, 2014, **118**, 22368-22372.
27. Z. Wang, H. Jia, X. Zheng, et al., *Nanoscale*, 2014, DOI: 10.1039/C1034NR04829F.
28. M. Buscema, D. J. Groenendijk, G. A. Steele, H. S. J. van der Zant and A. Castellanos-Gomez, *Nat. Commun.*, 2014, **5**, 4651.
29. H. Wang, X. Wang, F. Xia, et al., *Nano Lett.*, 2014, DOI: 10.1021/nl5029717.
30. M. Engel, M. Steiner and P. Avouris, *Nano Lett.*, 2014, DOI: 10.1021/nl502928y.
31. H. Liu, Y. Du, Y. Deng and P. D. Ye, *Chem. Soc. Rev.*, 2015, DOI: 10.1039/C1034CS00257A.
32. H. Fang, M. Tosun, G. Seol, T. C. Chang, K. Takei, J. Guo and A. Javey, *Nano Lett.*, 2013, **13**, 1991-1995.
33. A. Javey, R. Tu, D. B. Farmer, J. Guo, R. G. Gordon and H. Dai, *Nano Lett.*, 2005, **5**, 345-348.
34. J. Sun, G. Y. Zheng, H. W. Lee, et al., *Nano Lett.*, 2014, **14**, 4573-4580.
35. Q. Tang, Z. Zhou and Z. F. Chen, *Nanoscale*, 2013, **5**, 4541-4583.
36. T. Yildirim and S. Ciraci, *Phys. Rev. Lett.*, 2005, **94**, 175501.
37. M. Yoon, S. Y. Yang, C. Hicke, E. Wang, D. Geohegan and Z. Y. Zhang, *Phys. Rev. Lett.*, 2008, **100**, 206806.
38. Q. Sun, P. Jena, Q. Wang and M. Marquez, *J. Am. Chem. Soc.*, 2006, **128**, 9741-9745.
39. M. A. Zhou, Y. H. Lu, C. Zhang and Y. P. Feng, *Appl. Phys. Lett.*, 2010, **97**, 103109.
40. Y. H. Lu, M. Zhou, C. Zhang and Y. P. Feng, *J. Phys. Chem. C*, 2009, **113**, 20156-20160.
41. M. Zhou, Y. H. Lu, Y. Q. Cai, C. Zhang and Y. P. Feng, *Nanotechnology*, 2011, **22**, 385502.
42. F. Li, J. Zhao and Z. Chen, *J. Phys. Chem. C*, 2011, **116**, 2507-2514.
43. Y. D. Ma, Y. Dai, M. Guo, C. W. Niu, L. Yu and B. B. Huang, *Nanoscale*, 2011, **3**, 2301-2306.
44. Y. D. Ma, Y. Dai, M. Guo, C. W. Niu, J. B. Lu and B. B. Huang, *Phys. Chem. Chem. Phys.*, 2011, **13**, 15546-15553.
45. Y. D. Ma, Y. Dai, C. W. Niu and B. B. Huang, *J. Mater. Chem.*, 2012, **22**, 12587-12591.
46. P. Giannozzi, S. Baroni, N. Bonini, et al., *J. Phys.-Condes. Matter*, 2009, **21**, 19.
47. P. E. Blochl, *Phys. Rev. B*, 1994, **50**, 17953-17979.
48. J. P. Perdew, K. Burke and M. Ernzerhof, *Phys. Rev. Lett.*, 1996, **77**, 3865-3868.
49. G. Henkelman, A. Arnaldsson and H. Jonsson, *Comput. Mater. Sci.*, 2006, **36**, 354-360.
50. Y. L. Du, C. Y. Ouyang, S. Q. Shi and M. S. Lei, *J. Appl. Phys.*, 2010, **107**, 093718.
51. B. Shan and K. Cho, *Phys. Rev. Lett.*, 2005, **94**, 236602.
52. J. Zhao, J. Han and J. P. Lu, *Phys. Rev. B*, 2002, **65**, 193401.
53. X. Fan, W. T. Zheng, J.-L. Kuo and D. J. Singh, *ACS Appl. Mater. Interfaces*, 2013, **5**, 7793-7797.
54. Y. Liu, V. I. Artyukhov, M. Liu, A. R. Harutyunyan and B. I. Yakobson, *J. Phys. Chem. Lett.*, 2013, **4**, 1737-1742.
55. D. Y. Pan, S. Wang, B. Zhao, M. H. Wu, H. J. Zhang, Y. Wang and Z. Jiao, *Chem. Mater.*, 2009, **21**, 3136-3142.
56. H. Wang, C. Zhang, Z. Liu, et al., *J. Mater. Chem.*, 2011, **21**, 5430-5434.
57. W. Yuan, Y. Zhou, Y. Li, et al., *Sci. Rep.*, 2013, **3**, 2248.
58. A. V. Krasheninnikov, P. O. Lehtinen, A. S. Foster, P. Pyykko and R. M. Nieminen, *Phys. Rev. Lett.*, 2009, **102**, 126807.
59. H. Sevincli, M. Topsakal, E. Durgun and S. Ciraci, *Phys. Rev. B*, 2008, **77**, 195434.
60. K. T. Chan, J. B. Neaton and M. L. Cohen, *Phys. Rev. B*, 2008, **77**, 235430.
61. H. Valencia, A. Gil and G. Frapper, *J. Phys. Chem. C*, 2010, **114**, 14141-14153.
62. Y. Yagi, T. M. Briere, M. H. F. Sluiter, V. Kumar, A. A. Farajian and Y. Kawazoe, *Phys. Rev. B*, 2004, **69**, 075414.
63. T. O. Wehling, A. V. Balatsky, M. I. Katsnelson, A. I. Lichtenstein and A. Rosch, *Phys. Rev. B*, 2010, **81**, 115427.
64. D. Jacob and G. Kotliar, *Phys. Rev. B*, 2010, **82**, 085423.
65. W. Z. Li, C. H. Liang, W. J. Zhou, J. S. Qiu, Z. H. Zhou, G. Q. Sun and Q. Xin, *J. Phys. Chem. B*, 2003, **107**, 6292-6299.
66. M. H. Seo, S. M. Choi, H. J. Kim and W. B. Kim, *Electrochem. Commun.*, 2011, **13**, 182-185.
67. Y. Zhang, N. W. Franklin, R. J. Chen and H. J. Dai, *Chem. Phys. Lett.*, 2000, **331**, 35-41.
68. E. Hüger and K. Osuch, *EPL*, 2005, **71**, 276.
69. I. Gierz, C. Riedl, U. Starke, C. R. Ast and K. Kern, *Nano Lett.*, 2008, **8**, 4603-4607.
70. J. Zhao, A. Buldum, J. Han and J. P. Lu, *Phys. Rev. Lett.*, 2000, **85**, 1706-1709.
71. X. Lin and J. Ni, *Phys. Rev. B*, 2012, **86**, 075440.
72. E. Akturk, C. Ataca and S. Ciraci, *Appl. Phys. Lett.*, 2010, **96**, 123112.
73. B. Cordero, V. Gomez, A. E. Platero-Prats, et al., *Dalton Trans.*, 2008, 2832-2838.
74. B. Gamoke, D. Neff and J. Simons, *J. Phys. Chem. A*, 2009, **113**, 5677-5684.
75. M. Topsakal and S. Ciraci, *Phys. Rev. B*, 2012, **86**, 205402.
76. Y. Wang and Y. Ding, *Phys. Status Solidi RRL*, 2013, **7**, 410-413.
77. L. Wang, K. Lee, Y.-Y. Sun, M. Lucking, Z. Chen, J. J. Zhao and S. B. Zhang, *ACS Nano*, 2009, **3**, 2995-3000.
78. A. Castellanos-Gomez, L. Vicarelli, E. Prada, et al., *2D Mater.*, 2014, **1**, 025001.
79. D. W. Boukhvalov and M. I. Katsnelson, *J. Phys.-Condes. Matter*, 2009, **21**.
80. O. V. Yazyev and L. Helm, *Phys. Rev. B*, 2007, **75**, 125408.
81. E. J. Duplock, M. Scheffler and P. J. D. Lindan, *Phys. Rev. Lett.*, 2004, **92**, 225502.
82. S. Chen, L. Brown, M. Levendorf, et al., *ACS Nano*, 2011, **5**, 1321-1327.
83. S. Yang, G. Li, Q. Zhu and Q. Pan, *J. Mater. Chem.*, 2012, **22**, 3420-3425.
84. V. V. Kulish, M.-F. Ng, O. I. Malyi, P. Wu and Z. Chen, *RSC Advances*, 2013, **3**, 8446-8453.
85. H. Sahin and F. M. Peeters, *Phys. Rev. B*, 2013, **87**, 085423.
86. V. O. Ozcelik and S. Ciraci, *J. Phys. Chem. C*, 2013, **117**, 26305-26315.